Low Beam Energy SEM

Electronic supplementary material The online version of this chapter (https://doi.org/10.1007/978-1-4939-6676-9_11) contains supplementary material, which is available to authorized users.

J. Goldstein et al., *Scanning Electron Microscopy and X-Ray Microanalysis*,
https://doi.org/10.1007/978-1-4939-6676-9_11

The incident beam energy is one of the most useful parameters over which the microscopist has control because it determines the lateral and depth sampling of the specimen properties by the critical imaging signals. The Kanaya–Okayama electron range varies strongly with the incident beam energy:

$$R_{K-O}\,(\mathrm{nm}) = \left(27.6\,A / Z^{0.89}\rho\right) E_0^{1.67} \qquad (11.1)$$

where A is the atomic weight (g/mol), Z is the atomic number, ρ is the density (g/cm^3), and E_0 (keV) is the incident beam energy, which is shown graphically in Fig. 11.1a–c.

11.1 What Constitutes "Low" Beam Energy SEM Imaging?

The rapid but continuous decrease of the range with E_0 shown in Fig. 11.1a raises the question, Where does "low" beam energy SEM imaging begin? That is, what value of E_0 constitutes the upper bound of "low" beam energy microscopy? As will be discussed below, useful SEM imaging can now be accomplished down to remarkably low arrival energies at the specimen surface, less than 100 eV. The upper bound for E_0 is arbitrary, but a reasonable limit is the value discussed in the "Low Beam Energy X-Ray Microanalysis" module, where it is found that $E_0 = 5$ keV is the lowest beam energy for which a useful characteristic X-ray peak can be excited for all elements of the periodic table, excepting H and He, which do not produce characteristic X-rays. Thus, the plot of the range for $E_0 \leq 5$ keV shown in Fig. 11.1b will be taken to define the range for low beam energy SEM.

11.2 Secondary Electron and Backscattered Electron Signal Characteristics in the Low Beam Energy Range

The characteristics of the secondary electron (SE) and backscattered electron (BSE) signals observed in conventional SEM imaging performed at high beam energy ($E_0 \geq 10$ keV) can be summarized as follows: (1) For most elements, $\eta > \delta$.

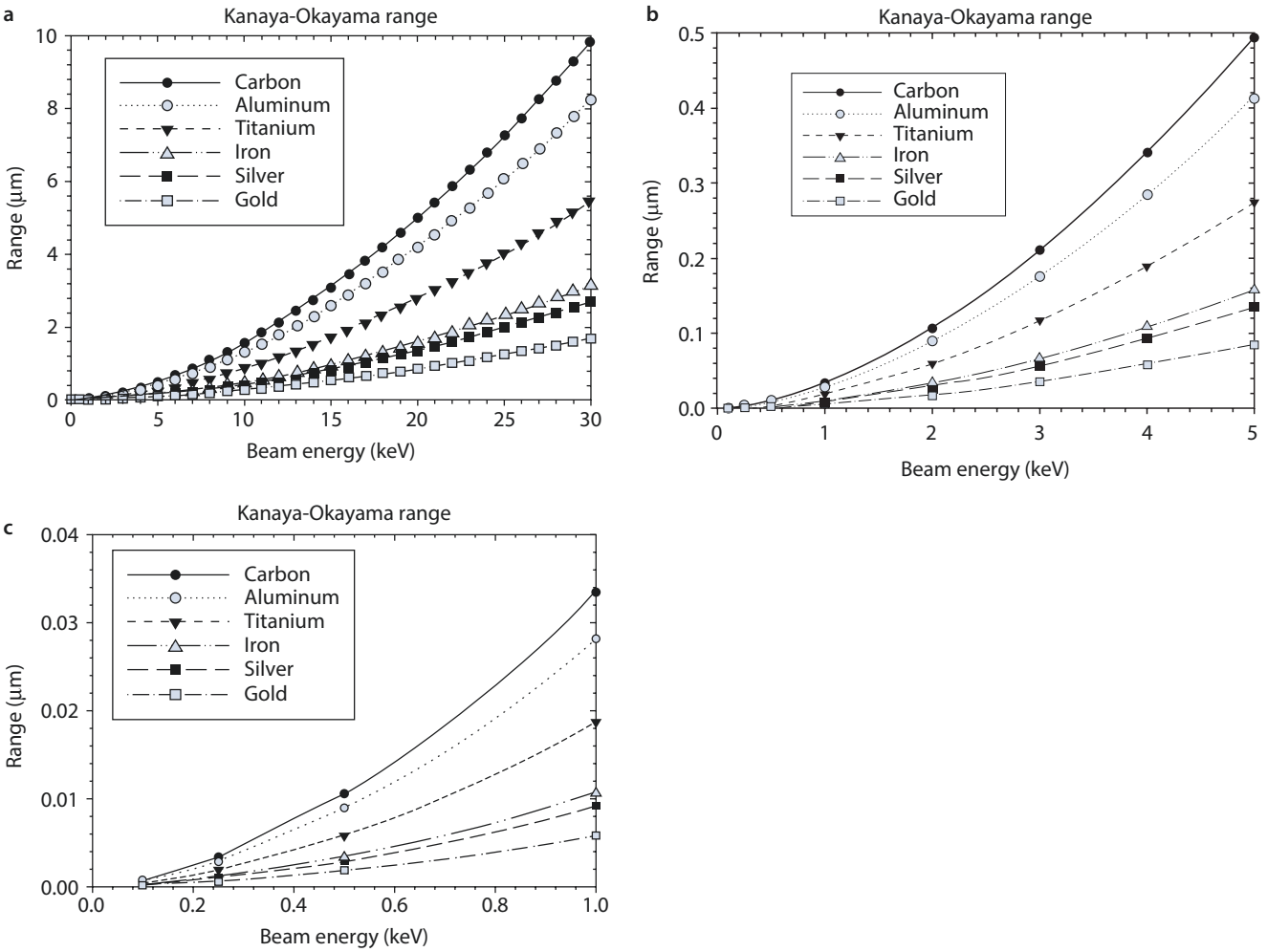

Fig. 11.1 Plot of the Kanaya–Okayama range for various elements: **a** 0–30 keV; **b** 0–5 keV; **c** 0–1 keV

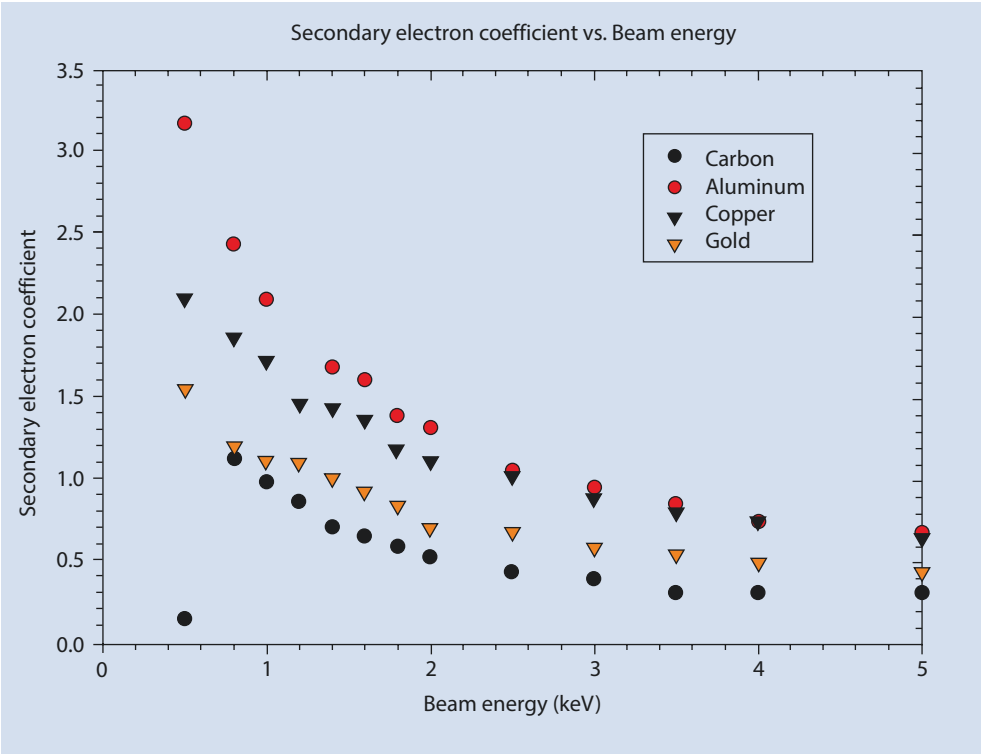

Fig. 11.2 Secondary electron coefficient, δ, as a function of beam energy for C, Al, Cu, and Au, taken from the data of Bongeler et al. (1993)

(2) Although the SE_1 are sensitive to surface characteristics within the escape depth of ~10 nm (metals), this surface sensitivity is diluted by the more numerous SE_2 and SE_3, which compose about 75–85 % of the total SE signal. SE_2 and SE_3 carry BSE information since they are created by the exiting BSEs at the specimen surface and on the chamber walls. Because the BSEs escape from approximately 15 % (high Z) to 30 % (low Z) of R_{K-O}, BSE depth sensitivity in turn determines the effective sampling of sub-surface information carried by the SE_2 and the SE_3, which is one to two orders of magnitude greater than the ~10 nm of the SE_1.

As E_0 is reduced into the low beam energy range below 5 keV, the rapid reduction in the electron range given by equation 11.1, as shown in Fig. 11.1 b, strongly influences the secondary electron coefficient: (1) The fraction of the incident energy lost by the beam electrons near the surface increases, which in turn increases the production of SEs, so that δ increases as the beam energy is reduced, as shown in Fig. 11.2 for several elements for measurements conducted in one laboratory. Because of this significant increase in SE production in the low beam energy range, generally $\delta > \eta$, as shown for Au in Fig. 11.3. In low beam energy SEM, backscattering still occurs, but due to their much greater abundance SEs generally dominate the signal collected by the Everhart–Thornley (E-T)(positive bias) detector. (2) As the beam energy decreases, the collapse of the lateral and depth ranges increases the fraction of the SE_2 and SE_3 that carry surface information equivalent to the SE_1. This trend makes the SE image increasingly sensitive to the surface characteristics of the material as the beam energy is reduced. However, the surface of a material is often unexpectedly complex. Upon exposure to the atmosphere, most "pure" elements form a thin surface oxide layer, for example, approximately 4 nm of Al_2O_3 forms on Al. Moreover, this surface layer may incorporate water chemically to form hydroxide and/or carbon dioxide to form carbonate, or there may be physical adsorption of these and other compounds from the environment which may not evaporate under vacuum. Additionally, there may be unexpected contamination from hydrocarbons deposited on the specimen surface which generally arise from the environment to which the specimen was exposed prior to the SEM. In some cases such contamination may be deposited from the SEM vacuum system if sufficient care has not been previously taken to eliminate sources of volatile contamination by rigorous specimen cleaning and by pre-pumping in an airlock prior to transferring into the specimen chamber. Complex surface composition is the likely reason for the wide range of δ values reported by various researchers measuring a nominally common target, as illustrated in Fig. 11.4 for aluminum, where reported values of δ span a factor of 4 or more. This is a common result across the periodic table, as seen in the SE database compiled by Joy (2012). The strong surface sensitivity of the SE and BSE signals at low beam energy to the condition of the specimen surface means that SEM image interpretation of "real" as-received specimens will be challenging. *In situ* cleaning by ion beam milling in a "dual beam" platform may

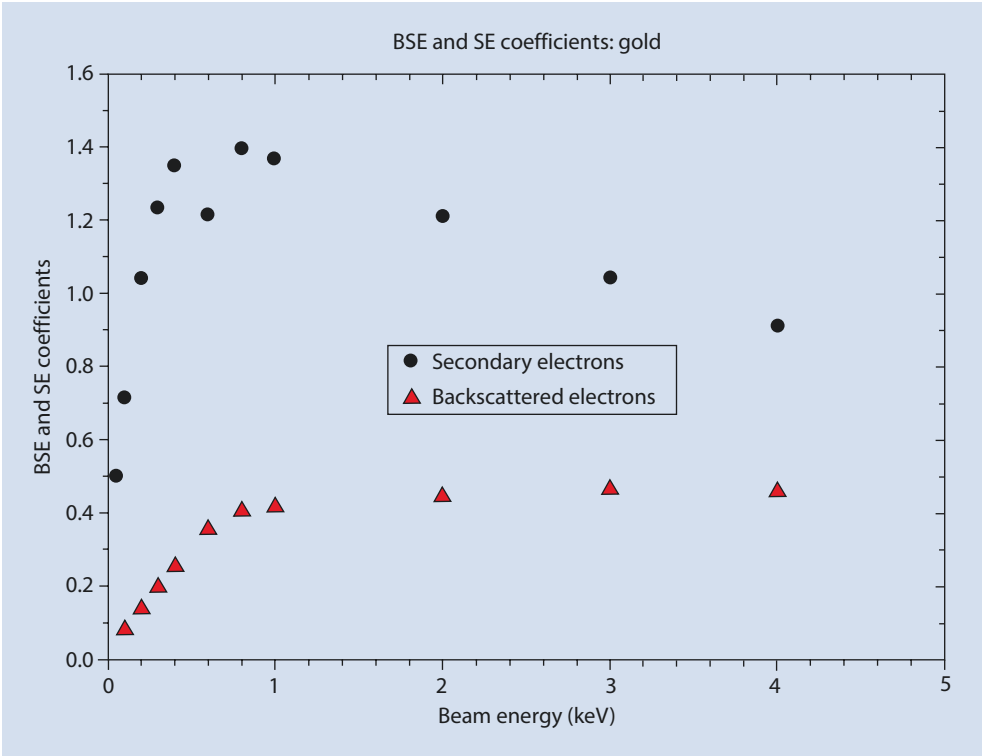

Fig. 11.3 Secondary electron coefficient, δ, and backscatter electron coefficient, η, as a function of beam energy for Au, taken from the data of Bongeler et al. (1993)

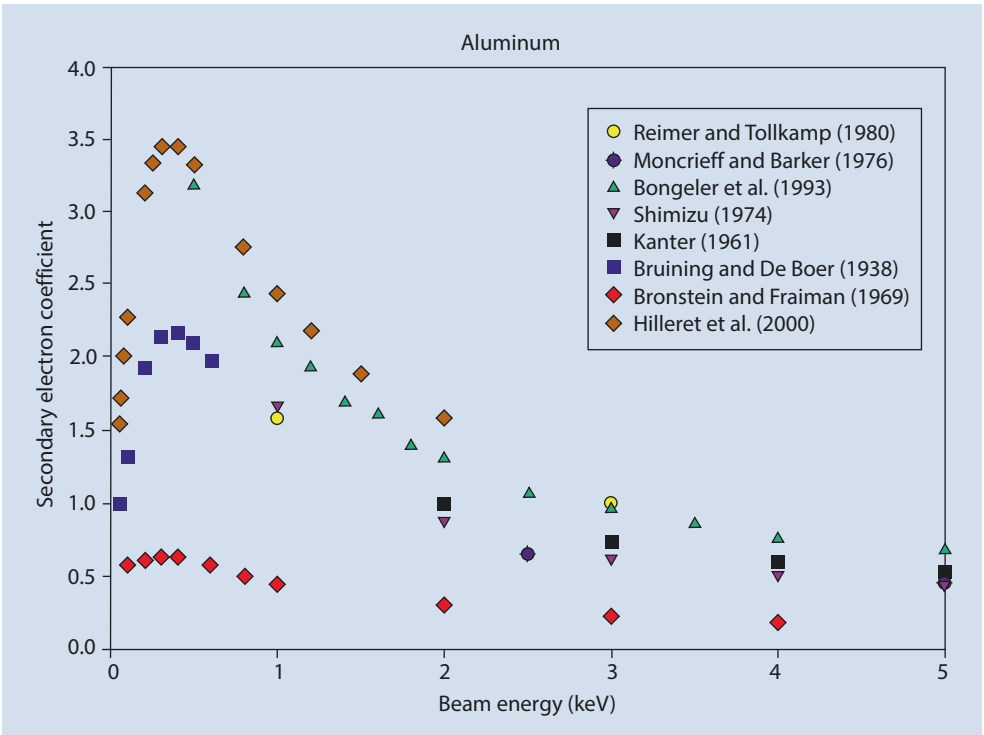

Fig. 11.4 Secondary electron coefficient, δ, as a function of beam energy for Al (Taken from the data of various authors)

remove such artifacts. However, even with ion beam cleaning, it must be recognized that at the vacuum levels of the conventional "high vacuum" SEM, for example, 10^{-4} Pa (10^{-6} torr), the partial pressure of oxygen is sufficiently high that a monolayer of oxide will form on a reactive surface such as Al in a matter of seconds. Thus, while ion beam milling may successfully remove contamination, oxide formation at least at the monolayer level may be unavoidable

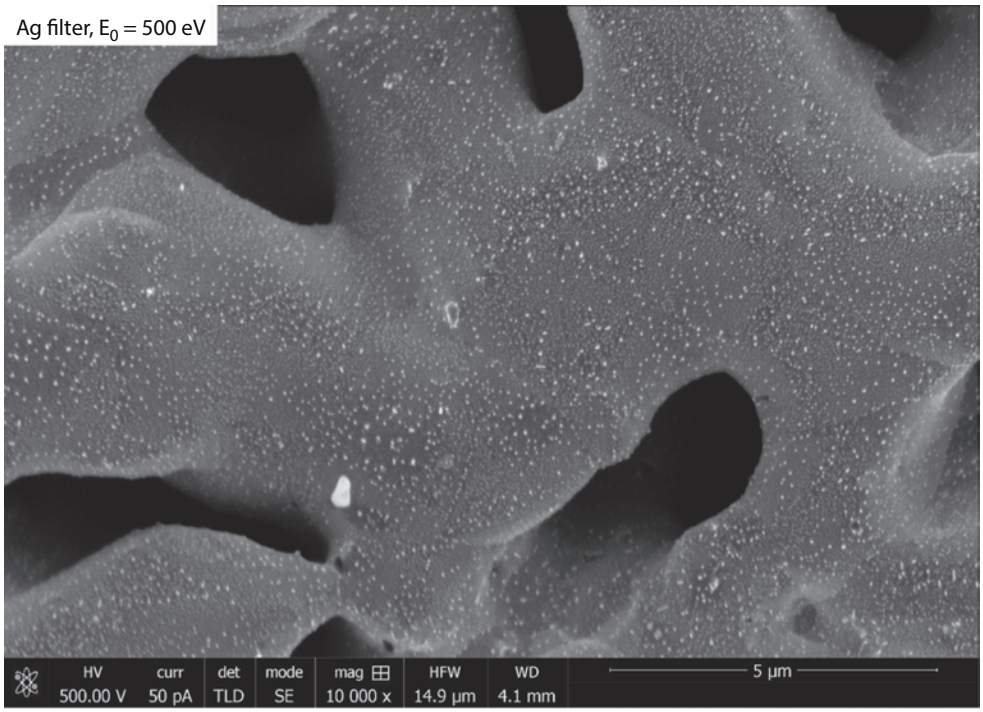

Fig. 11.5 SEM image of a silver filter obtained at $E_0 = 0.5$ keV with a through-the-lens secondary electron detector; Bar = 5 µm (Image courtesy of Keana Scott, NIST)

unless an ultrahigh vacuum instrument is used, where the chamber pressure is $<10^{-8}$ Pa (10^{-10} torr).

11.3 Selecting the Beam Energy to Control the Spatial Sampling of Imaging Signals

11.3.1 Low Beam Energy for High Lateral Resolution SEM

The electron range controls the lateral spatial distribution of the backscattered electrons: 90 % of BSEs escape radially from approximately 30 % $R_{K\text{-}O}$ (high Z) to 60 % $R_{K\text{-}O}$ (low Z). The lateral spatial distribution of the SE_2, which is created as the BSE escape through the surface, and the SE_3, which is the BSE-to-SE conversion signal that results when BSE strike the objective lens pole piece, the stage components, and the chamber walls, effectively sample the same spatial range as the BSE. As the incident beam energy is lowered, the BSE (SE_3) and SE_2 signal lateral distributions collapse onto the SE_1 distribution, which is restricted to the beam footprint, so that at sufficiently low beam energy all of these signals carry high spatial resolution information similar to the SE_1. With a modern high performance SEM equipped with a high brightness source, for example, a cold field emission gun or a Schottky thermally assisted field emission gun, capable of delivering a useful beam current into a nanometer or sub-nanometer diameter beam, low beam energy SEM operation has become the most frequent choice to achieve high lateral spatial resolution imaging of bulk specimens, as discussed in detail in the "High Resolution SEM" module. An example of high spatial resolution achieved at low beam energy is shown in Fig. 11.5 for a silver filter material imaged at $E_0 = 0.5$ keV with a "through-the-lens" secondary electron detector. Unfortunately, there is no simple rule like η vs. Z at high beam energy for interpreting the contrast seen in this image. For example, why does the population of nanoscale particles appear extremely bright against the general mid-level gray of the bulk background of the silver structure. These features may appear bright because of local compositional differences such as thicker oxides or there may be a physical change such as increased surface area for SE emission due to nanoscale roughening.

11.3.2 Low Beam Energy for High Depth Resolution SEM

The strong exponential dependence of the beam penetration on the incident energy controls the sampling of sub-surface specimen properties by the BSEs and SEs, which can provide insight on the depth dimension. Observing a specimen as the beam energy is progressively lowered to record systematic changes can reveal lateral heterogeneities in surface composition. Fig. 11.6 shows such a sequence of images from high beam energy (30 keV) to low beam energy (1 keV) prepared with an E–T(positive bias) detector where the specimen is an aluminum stub upon which was deposited approximately

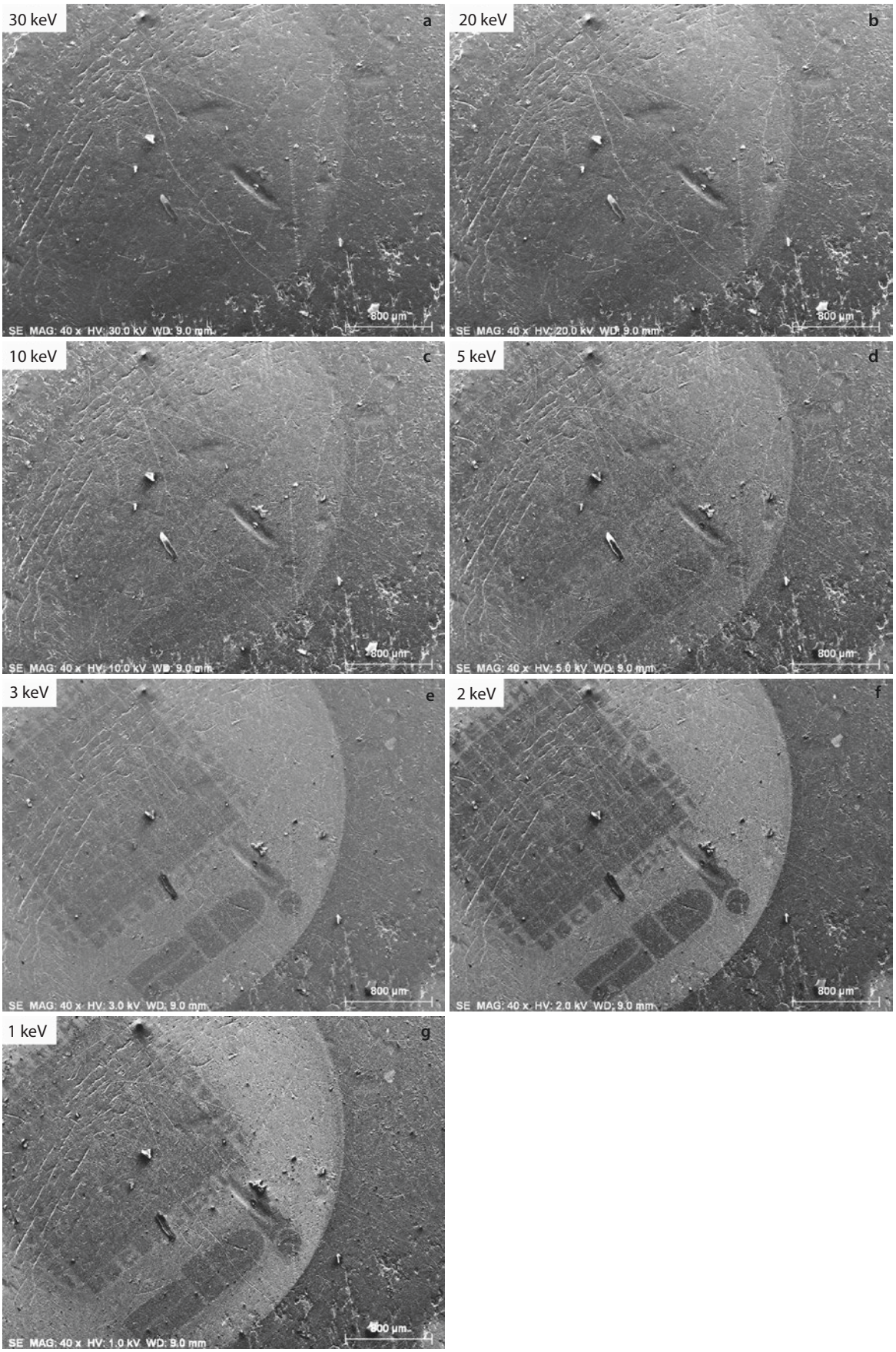

Fig. 11.6 Beam energy series of images of a carbon film, nominally 7 nm thick, deposited on an aluminum SEM stub in the as-received condition prepared with an E–T(positive bias) detector: **a** 30 keV; **b** 20 keV; **c** 10 keV; **d** 5 keV; **e** 3 keV; **f** 2 keV; **g** 1 keV; Bar = 800 µm

7 nm of carbon shadowed through a grid. The contrast between the carbon and the aluminum behaves in a complex fashion. The C-Al contrast is only weakly visible above $E_0 = 5$ keV despite a high electron dose, long image integration, and post-acquisition image processing for contrast enhancement. The C-Al contrast increases sharply as the beam energy decreases below 5 keV, reaching a maximum at $E_0 = 2$ keV and then decreasing below this energy. The increase in contrast below 5 keV is consistent with the increasing separation between the values of δ for C and Al seen in Fig. 11.2. The eventual decrease in the C-Al contrast below $E_0 = 2$ keV is not consistent with the measurements plotted in Fig. 11.2, where the difference between δ for C and Al actually increases below $E_0 = 2$ keV, which should increase the contrast. Despite the difficulty in interpreting these trends in contrast, this example demonstrates that lateral differences in the surface can be detected, provided care is taken to fully explore the image response to changing the beam energy parameter.

11.3.3 Extremely Low Beam Energy Imaging

High performance SEMs typically operate down to beam energies below 0.5 keV, with the lower limit depending on the vendor and the particular model. Ultralow beam energies below 0.1 keV can be achieved through different electron-optical techniques, including biasing the specimen to –V. Specimen biasing acts to decelerate the beam electrons emitted at energy E_0 from the column so that the landing energy, that is, the kinetic energy remaining when the beam electrons reach the specimen surface, is E_0 –eV, where e represents the electronic charge. Ultralow beam energy imaging is illustrated in Fig. 11.7, where the surface of a silica (SiO_2) specimen is imaged at a landing energy of 0.030 keV (30 eV). Figure 11.8 shows gold islands on carbon imaged with a landing energy of 0.01 keV (10 eV). At such low incident energy, only the outermost atomic/molecular layers are probed by the beam.

Fig. 11.7 Extremely low landing energy ($E_0 = 0.030$ keV) SEM image of silica (SiO_2) prepared with an Everhart-Thornley E–T(positive bias) detector and a beam current of 250 pA revealing fine-scale texture and surface topography; Bar = 2 µm (Image courtesy of Carl Zeiss)

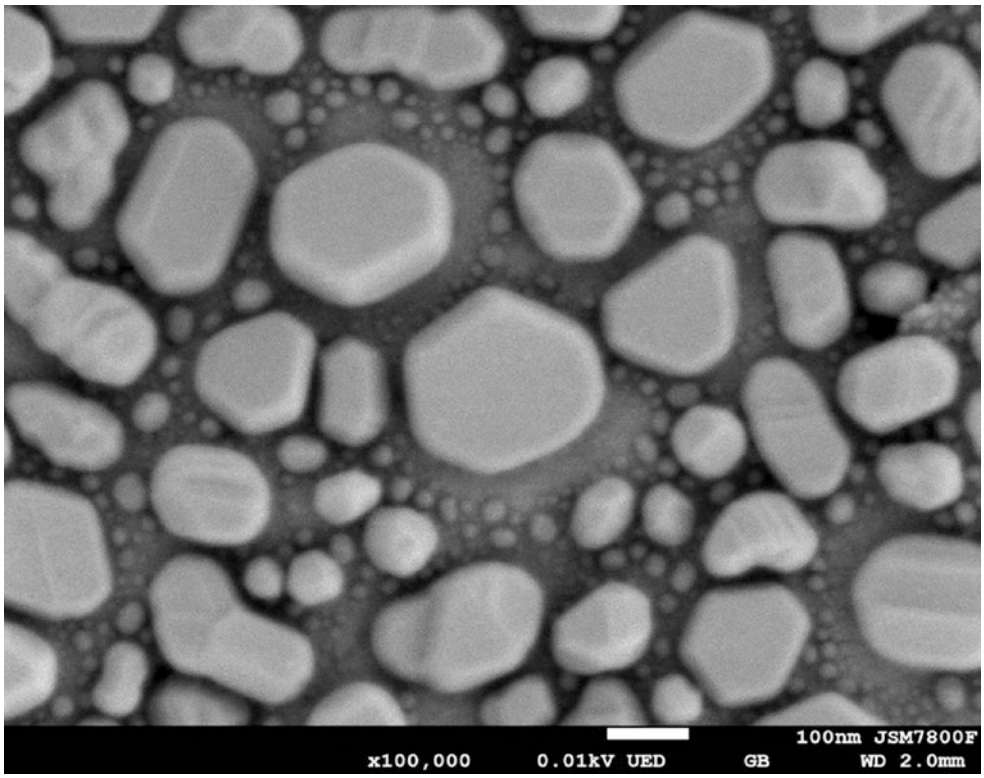

Fig. 11.8 Extremely low landing energy ($E_0 = 0.010$ keV) image of gold islands evaporated on carbon; TTL SE detector; Bar = 100 nm (Image courtesy of V. Robertson, JEOL)

References

Bongeler R, Golla U, Kussens M, Reimer L, Schendler B, Senkel R, Spranck M (1993) Electron-specimen interactions in low-voltage scanning electron microscopy. Scanning 15:1

Bronstein IM, Fraiman BS (1969) "Secondary electron emission" Vtorichnaya elektronnaya emissiya. Nauka, Moskva, p 340

Bruining H, De Boer JM (1938) Secondary electron emission: Part 1 secondary electron emission of metals. Phys Ther 5:17p

Hilleret N, Bojko J, Grobner O, Henrist B, Scheuerlein C, and Taborelli M (2000) "The secondary electron yield of technical materials and its Variation with surface treatments" in Proc.7th European Particle Accelerator Conference, Vienna

Joy D (2012) Can be found in chapter 3 on SpringerLink: http://link.springer.com/chapter/10.1007/978-1-4939-6676-9_3

Kanter M (1961) Energy dissipation and secondary electron emission in solids. Phys Rev 121:1677

Moncrieff DA, Barker PR (1976) Secondary electron emission in the scanning electron microscope. Scanning 1:195

Reimer L, Tolkamp C (1980) Measuring the backscattering coefficient and secondary electron yield inside a scanning electron microscope. Scanning 3:35

Shimizu R (1974) Secondary electron yield with primary electron beam of keV. J Appl Phys 45:2107